BEILSTEIN JOURNAL OF NANOTECHNOLOGY

Supporting Information

for

Exploring combinations of spatial laser beam shaping for advancing nanoparticle synthesis by ablation in liquids

Rémi Bérard, Abdel Rahman Altakroury, Oleksandr Gatsa, Zongwen Fu, Bilal Gökce and Alexander V. Bulgakov

Beilstein J. Nanotechnol. **2026,** *17,* 1605–1623. doi:10.3762/bjnano.17.110

Additional experimental data and figures

License and Terms: This is a supporting information file under the terms of the Creative Commons Attribution License (https://creativecommons.org/licenses/by/4.0). Please note that the reuse, redistribution and reproduction in particular requires that the author(s) and source are credited and that individual graphics may be subject to special legal provisions.
The license is subject to the *Beilstein Journal of Nanotechnology* terms and conditions: (https://www.beilstein-journals.org/bjnano/terms)

SEM images of nanoparticles and size distributions

Here, we present representative SEM images of NPs obtained under all investigated PLAL conditions, along with their corresponding size distributions.

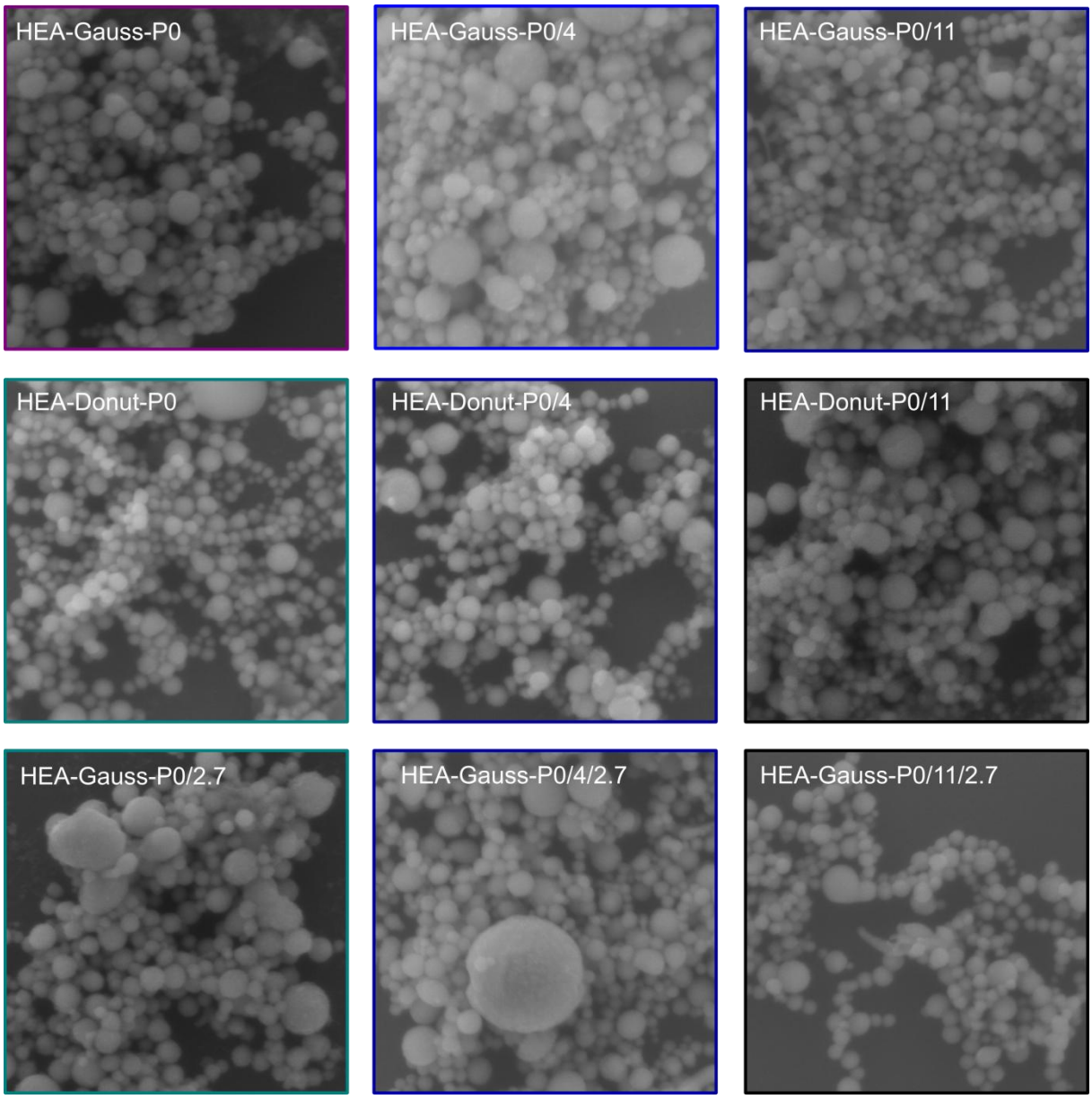


Figure S1: SEM images of HEA NPs produced by single-beam PLAL (Gaussian and donut) at different laser powers. For comparison convenience, two images are shown for one regime with Gaussian pulses at the same laser power indicated as P_0/4/2.7 and P_0/11. The frame size of the images is 1 × 1 μm.

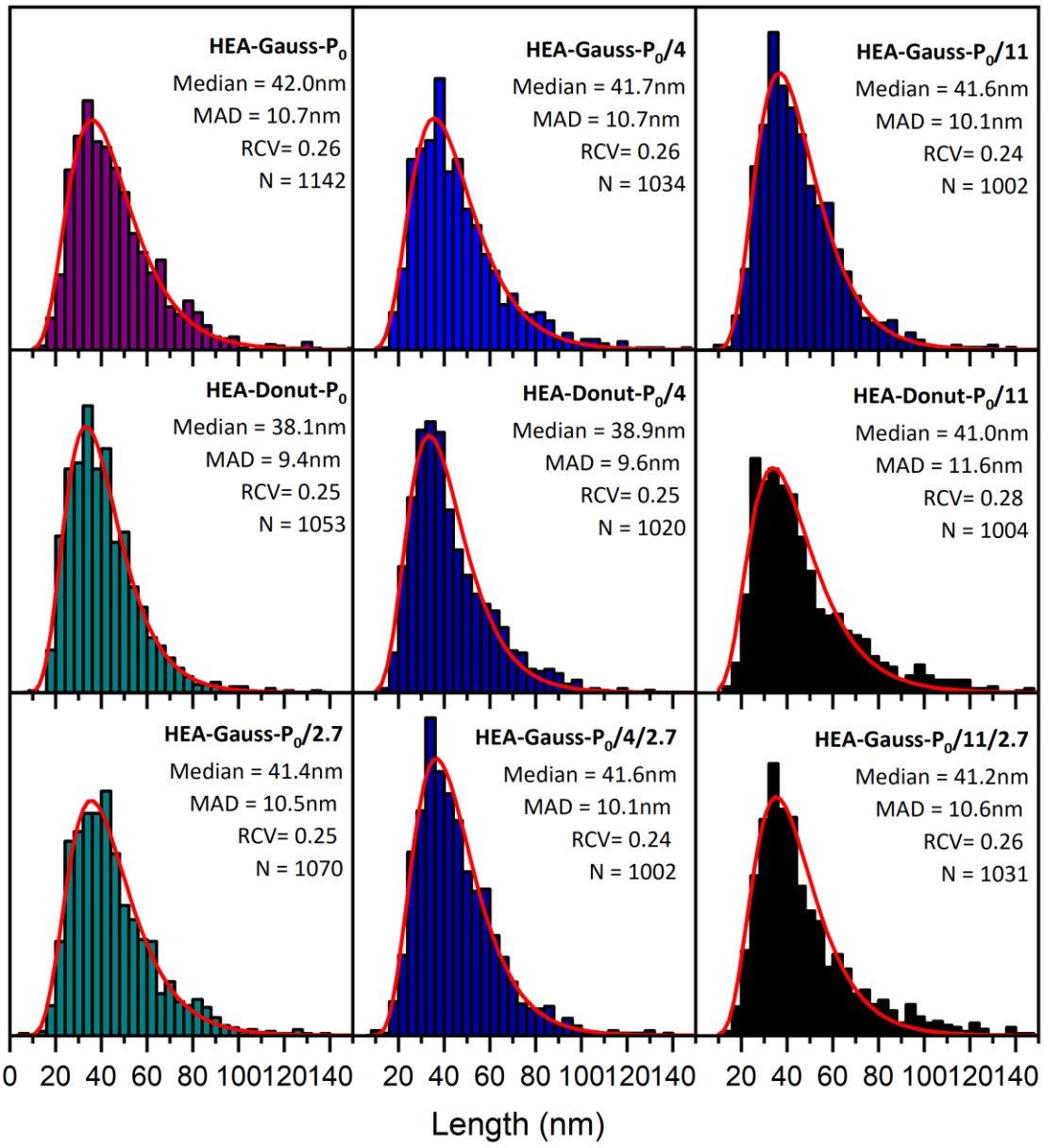


Figure S2: Size distributions of HEA NPs for single-beam PLAL (Gaussian and donut) corresponding to the images in Figure S1 and shown in Figure 2 of the article as violin plots. The statistical values indicated in each panel (median, MAD, and RCV) were calculated directly from the experimental particle-size data. For comparison convenience, one regime with Gaussian pulses is shown twice as P_0/4/2.7 and P_0/11.

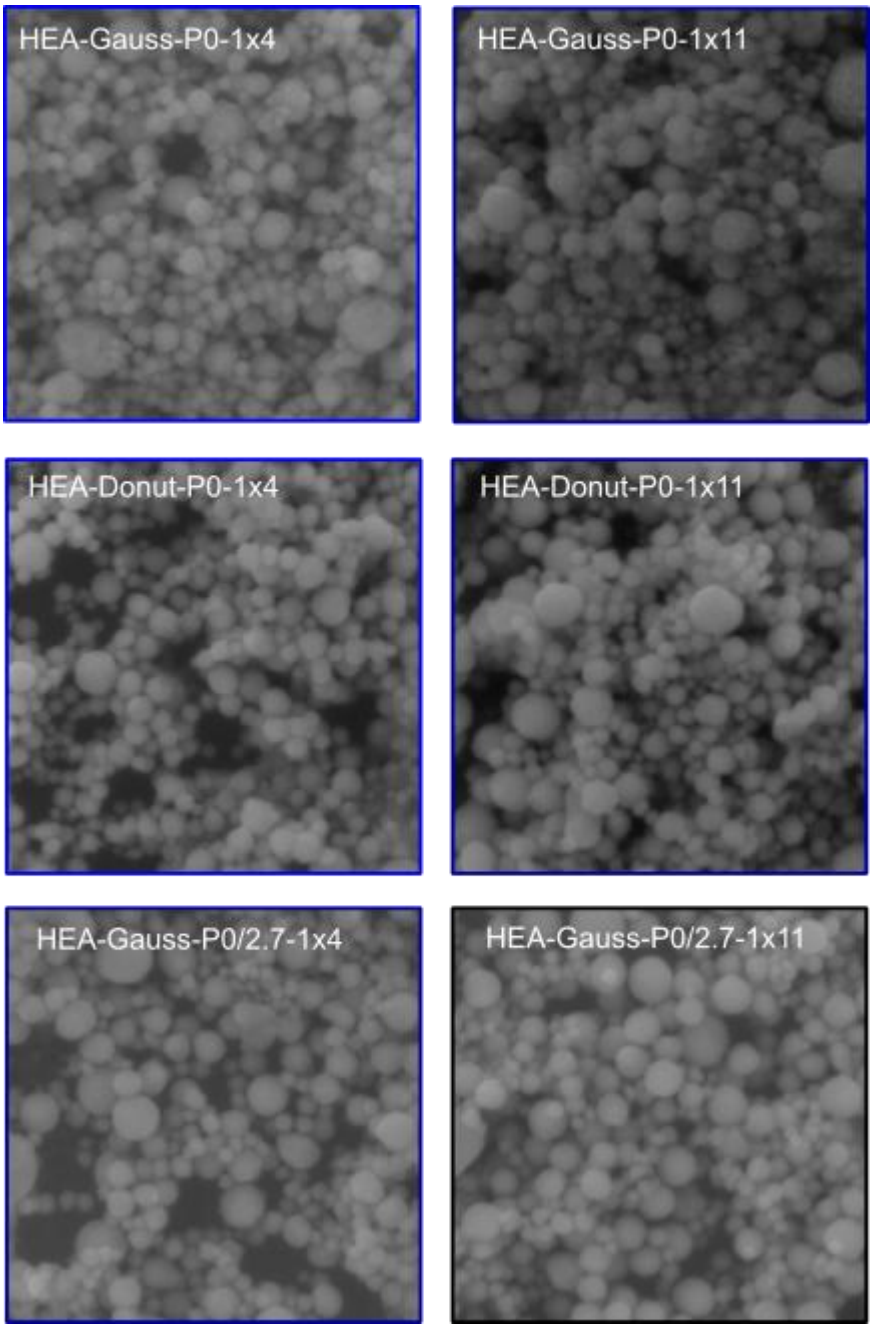


Figure S3: SEM images of HEA NPs produced by multi-beam PLAL (Gaussian and donut) at different DOEs and laser powers. The frame size of the images is 1 × 1 µm.

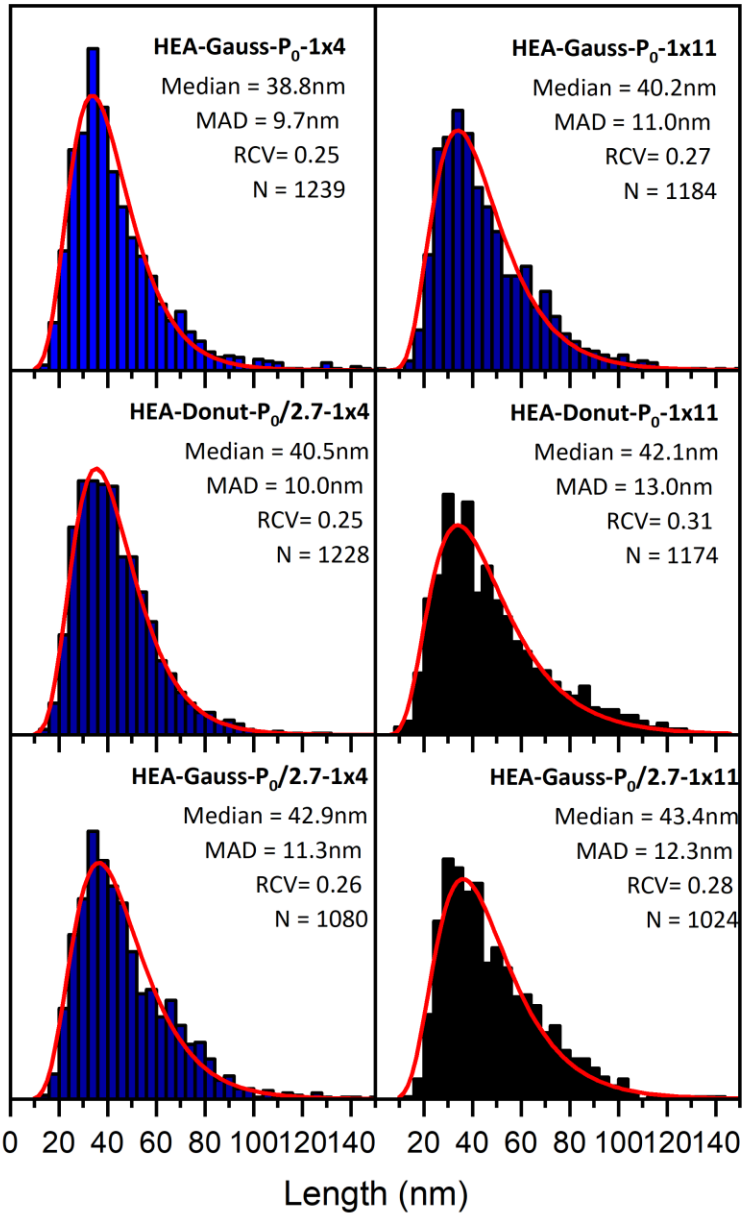


Figure S4: Size distributions of HEA NPs produced by multi-beam PLAL (Gauss and donut) corresponding to the images in Figure S3 and shown in Figure 2 of the article as violin plots. The statistical values indicated in each panel (median, MAD, and RCV) were calculated directly from the experimental particle-size data.

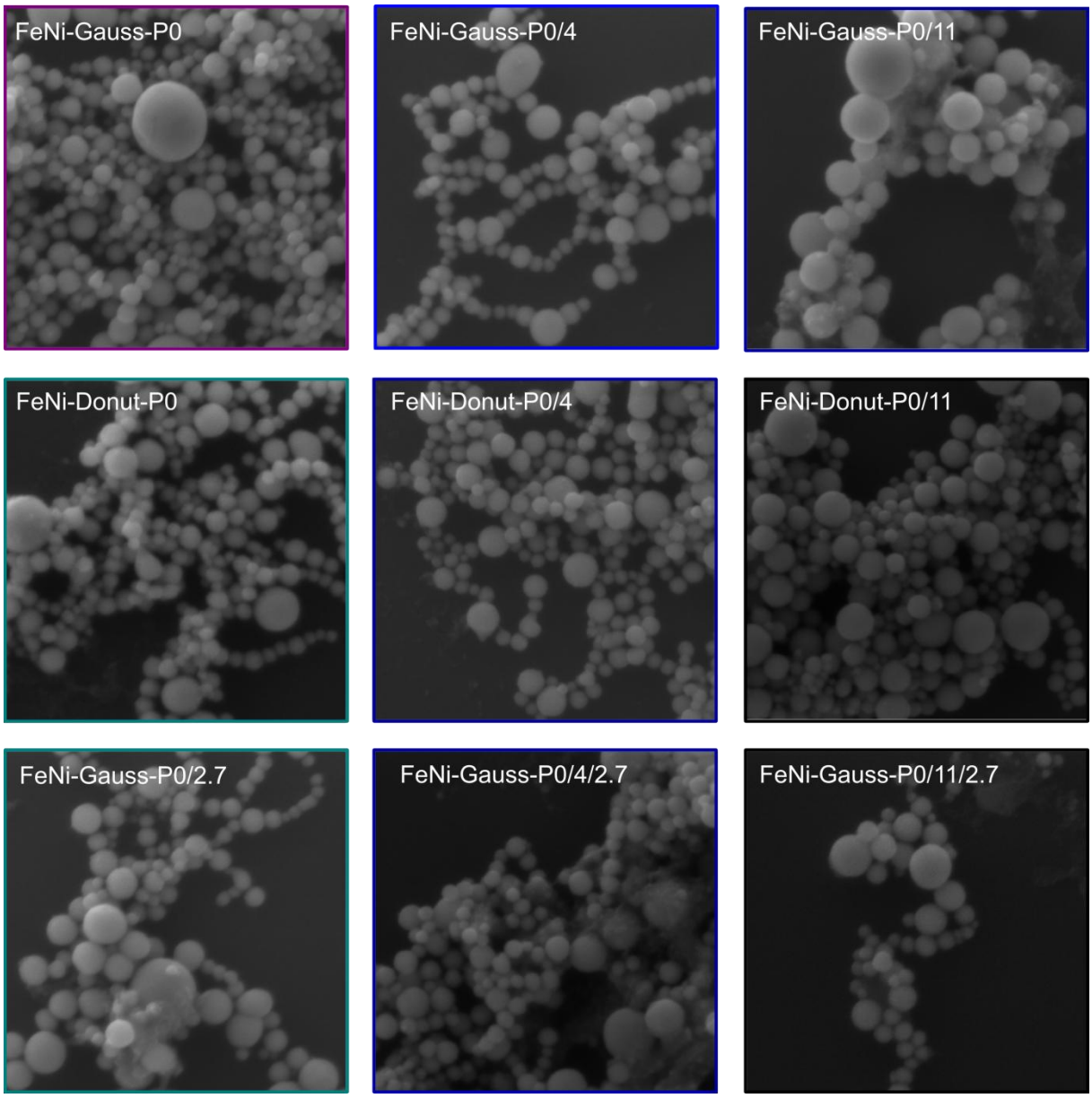


Figure S5: SEM images of FeNi NPs produced by single-beam PLAL (Gaussian and donut) at different laser powers. For comparison convenience, two images are shown for one regime with Gaussian pulses at the same laser power indicated as P_0/4/2.7 and P_0/11. The frame size of the images is 1 × 1 μm.

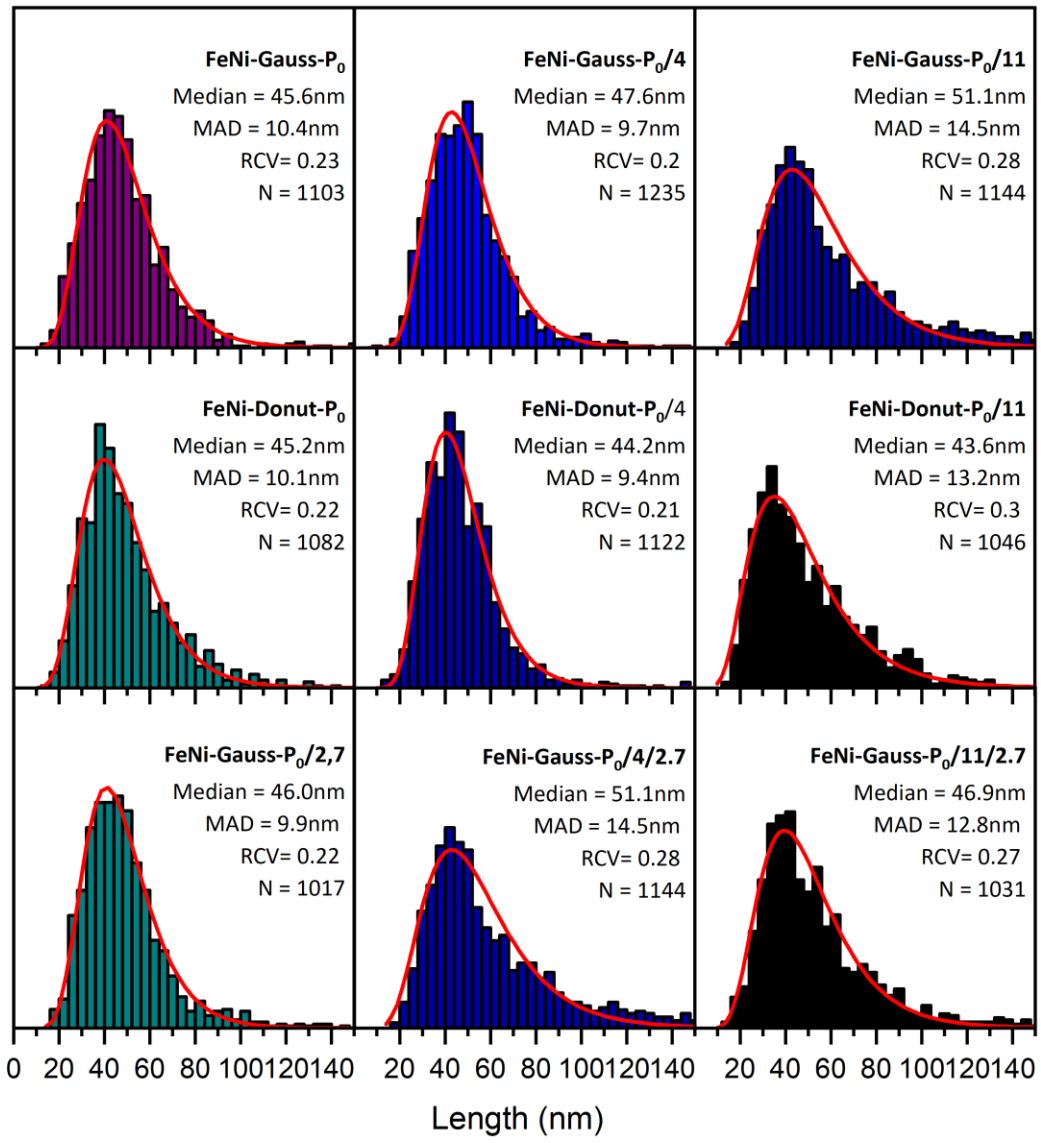


Figure S6: Size distributions of FeNi NPs for single-beam PLAL (Gaussian and donut) corresponding to the images in Figure S5 and shown in Figure 3 of the article as violin plots. The statistical values indicated in each panel (median, MAD, and RCV) were calculated directly from the experimental particle-size data. For comparison convenience, one regime with Gaussian pulses is shown twice as $P_0/4/2.7$ and $P_0/11$.

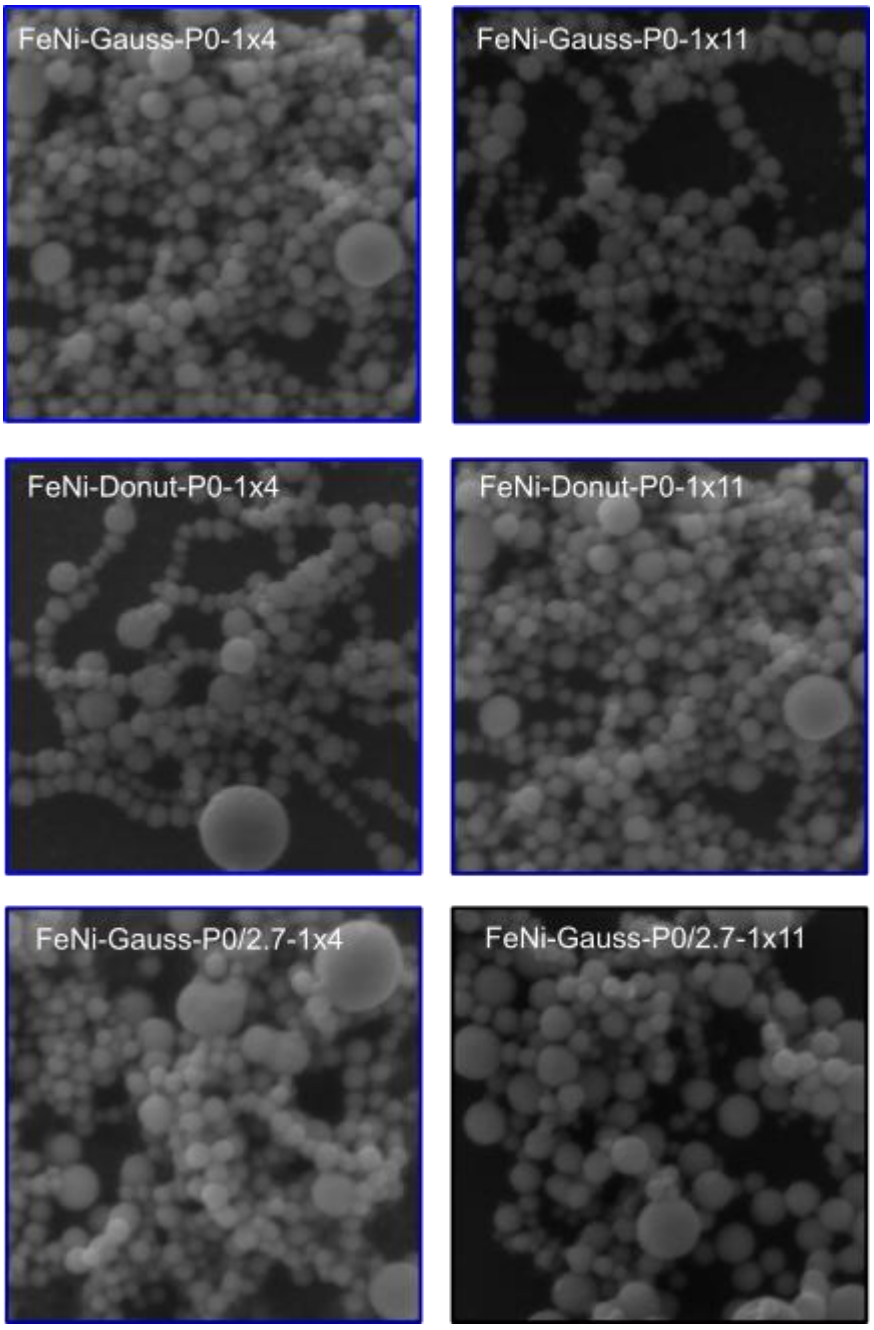


Figure S7: SEM images of FeNi NPs produced by multi-beam PLAL (Gaussian and donut) at different DOEs and laser powers. The frame size of the images is 1 × 1 µm.

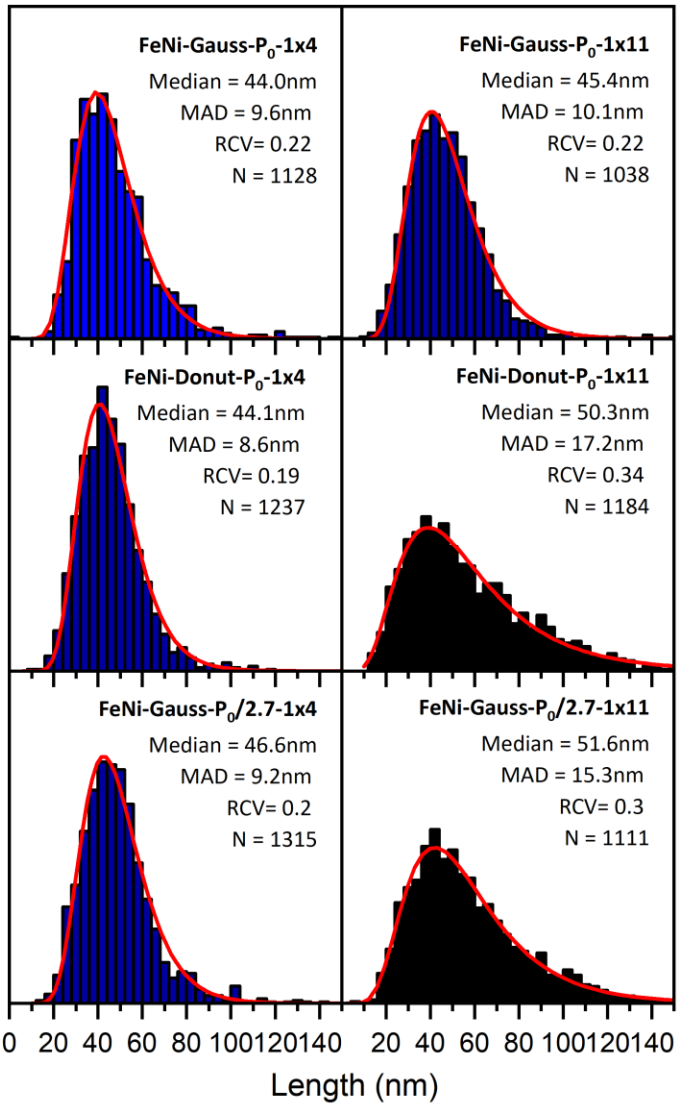


Figure S8: Size distributions of FeNi NPs produced by multi-beam PLAL (Gauss and donut) corresponding to the images in Figure S7 and shown in Figure 3 of the article as violin plots. The statistical values indicated in each panel (median, MAD, and RCV) were calculated directly from the experimental particle-size data.

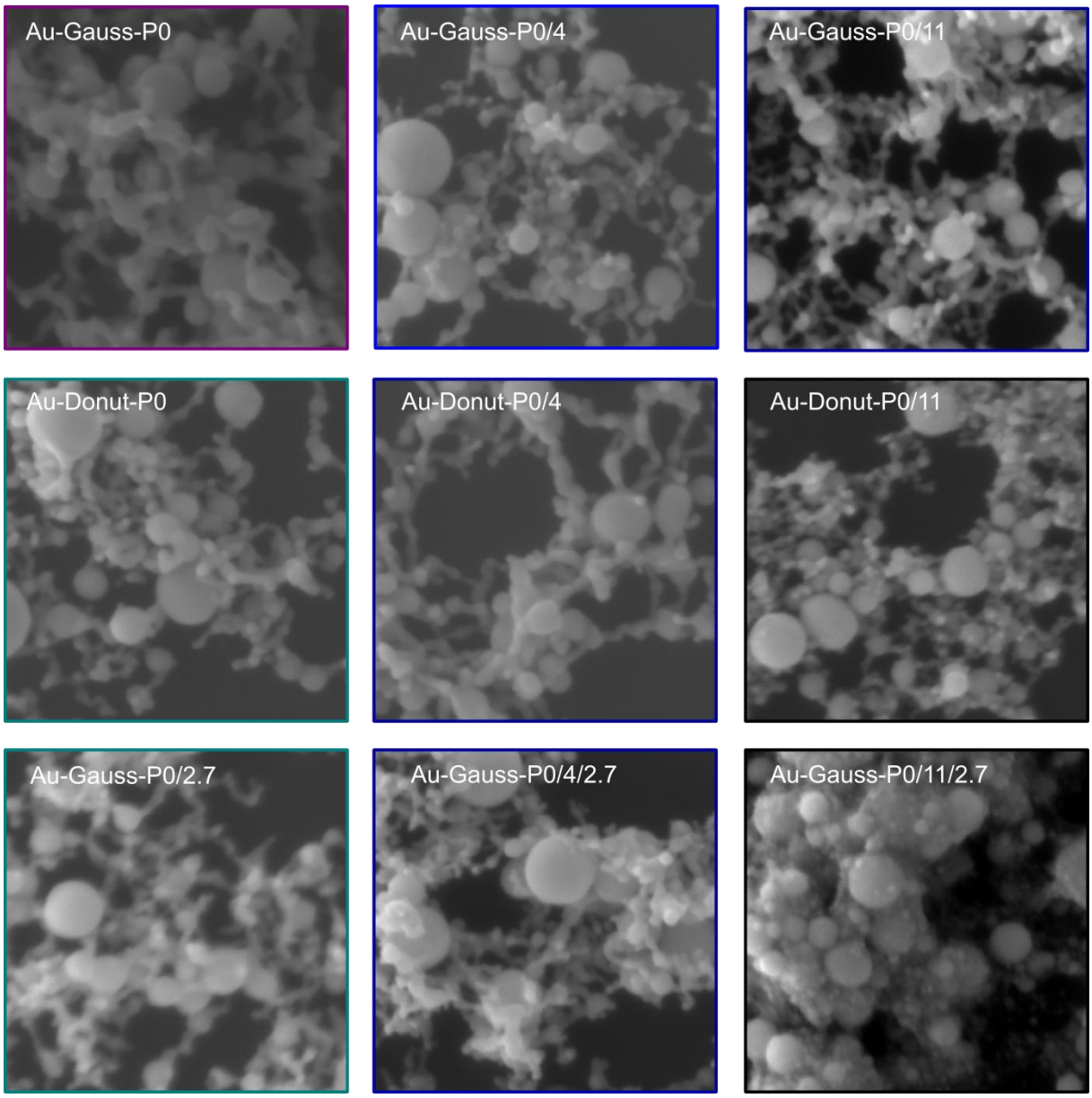


Figure S9: SEM images of Au NPs produced by single-beam PLAL (Gaussian and donut) at different laser powers. For comparison convenience, two images are shown for one regime with Gaussian pulses at the same laser power indicated as P_0/4/2.7 and P_0/11. The frame size of the images is 500 × 500 nm.

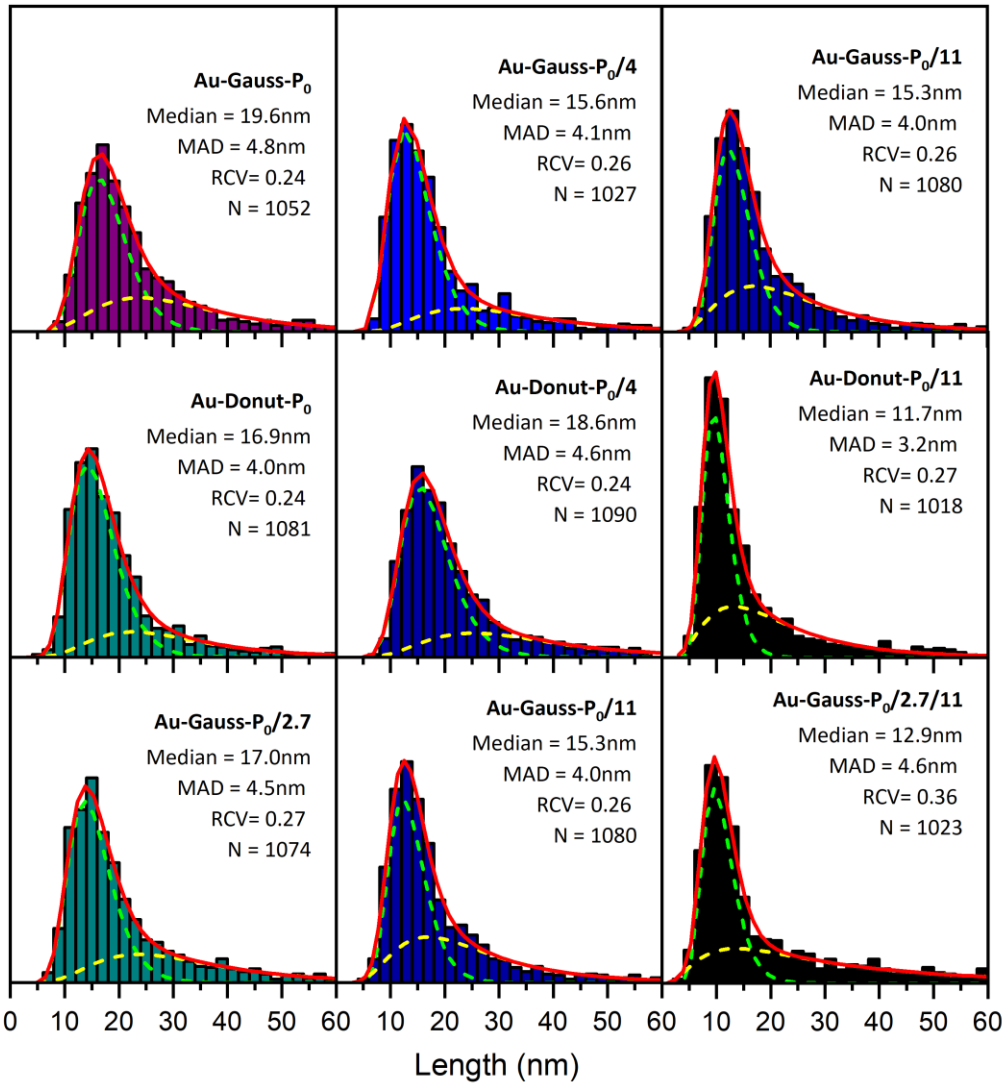


Figure S10: Size distributions of Au NPs for single-beam PLAL (Gaussian and donut) corresponding to the images in Figure S9 and shown in Figure 4 of the article as violin plots. The distributions are fitted by two lognormal functions for small (green dashed lines) and large (blue dashed lines) NP populations. The red lines represent combined fits. The statistical values indicated in each panel (median, MAD, and RCV) were calculated directly from the experimental particle-size data. For comparison convenience, one regime with Gaussian pulses is shown twice as P_0/4/2.7 and P_0/11.

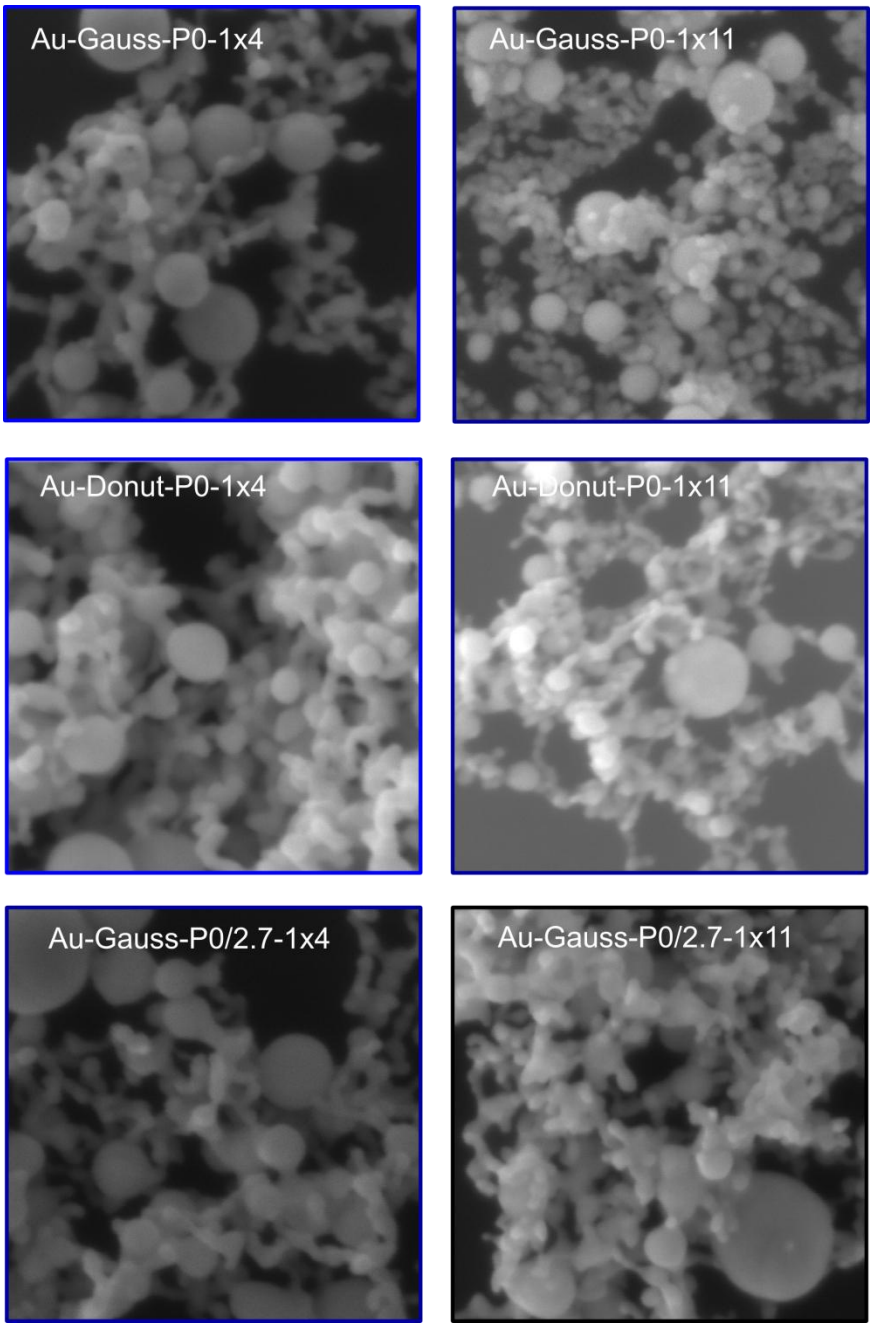


Figure S11: SEM images of Au NPs produced by multi-beam PLAL (Gaussian and donut) at different DOEs and laser powers. The frame size of the images is 500 × 500 nm.

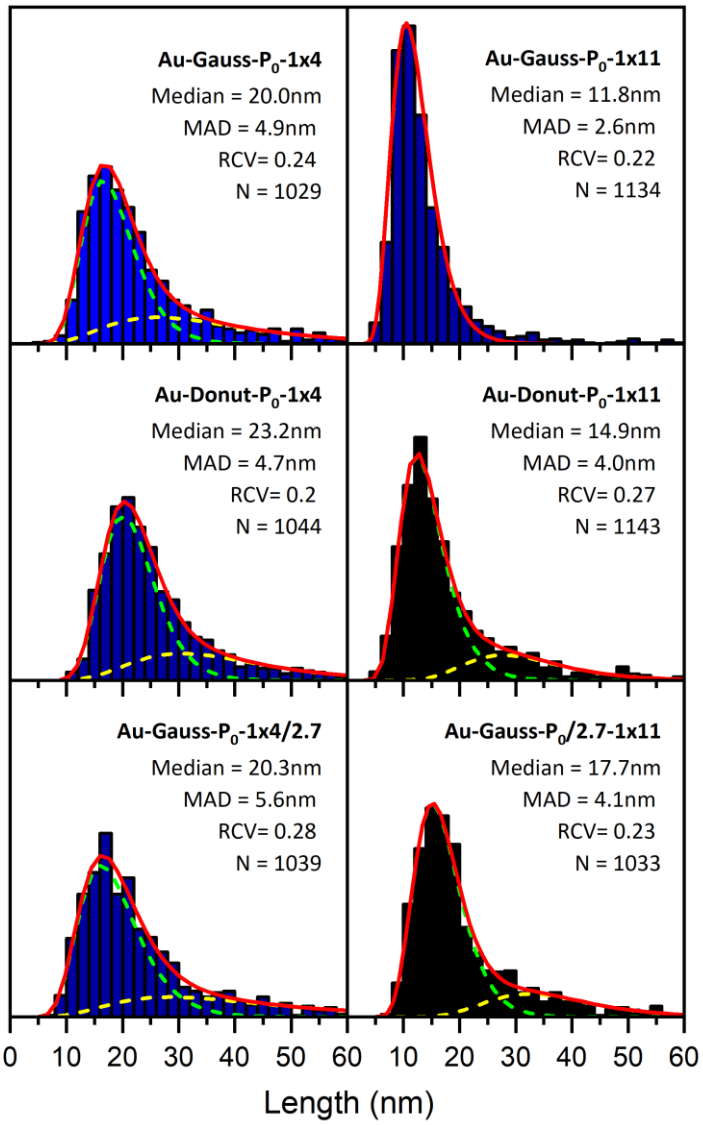


Figure S12: Size distributions of Au NPs for multi-beam PLAL (Gaussian and donut) corresponding to the images in Figure S11 and shown in Figure 4 of the article as violin plots. The distributions are fitted by two lognormal functions for small (green dashed lines) and large (blue dashed lines) NP populations. The red lines represent combined fits. The statistical values indicated in each panel (median, MAD, and RCV) were calculated directly from the experimental particle-size data.

PLAL system geometry with the 1×11 DOE

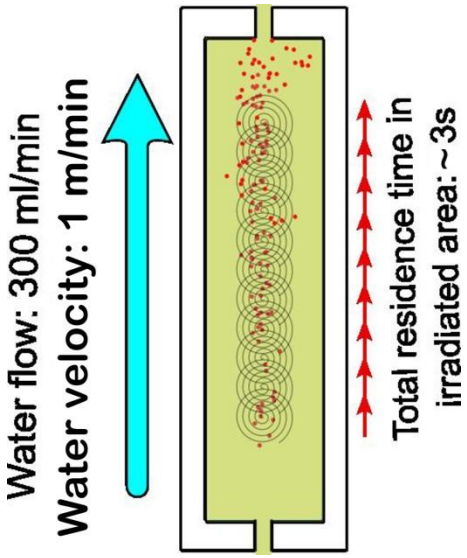


Figure S13: Schematic of the water flow and 11-beam spiral pattern illustrating how the irradiation geometry can promote repeated laser exposure of the produced nanoparticles and thereby favor their laser-induced fragmentation.

High-mass cut-off size

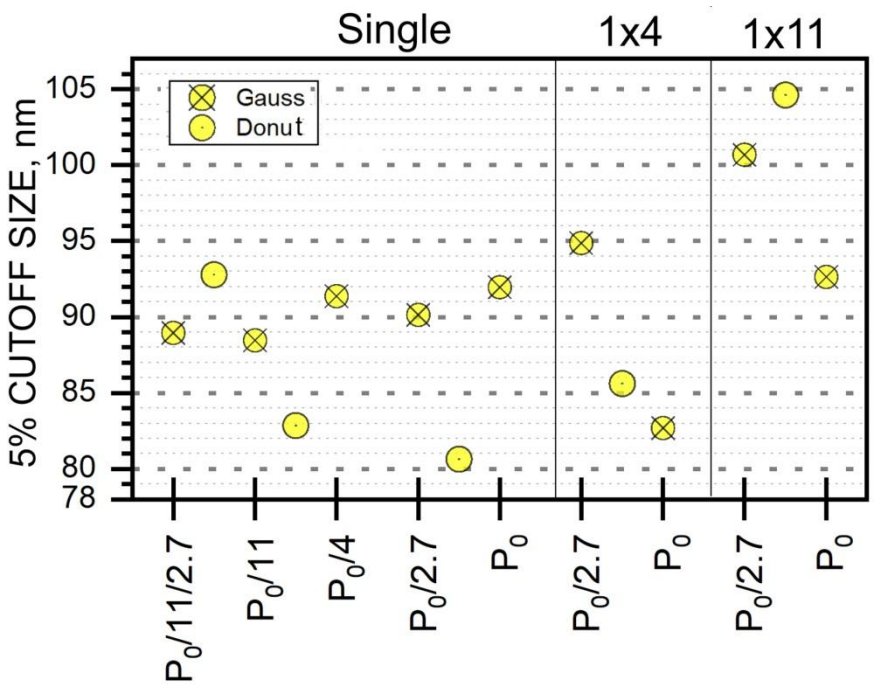


Figure S14: High-mass cut-off size of HEA NPs produced under different PLAL conditions with Gaussian and donut-shaped pulses. The cut-off is determined at a 5% of the NP probability density at the distribution tail from log-normal fittings. For convenience, the results for donut-shaped pulses obtained at a *P* power are placed between *P* and *P*/2.7 (the latter corresponds to the same fluence of a Gaussian pulse at *P*).